

# Thermomechanical Loading of Multilayered Cylindrical Geometries in Thermal Cycling from 300 to 1300 K

R. C. Hendricks and G. McDonald  
*Lewis Research Center*  
*Cleveland, Ohio*

and

R. L. Mullen  
*Case Western Reserve University*  
*Cleveland, Ohio*

and

M. J. Braun, B. T. Chung, and J. Padovan  
*University of Akron*  
*Akron, Ohio*

Prepared for the  
Thermal Engineering Joint Conference  
cosponsored by the American Society of Mechanical Engineers  
and the Japan Society of Mechanical Engineers  
Honolulu, Hawaii, March 20-24, 1983



THERMOMECHANICAL LOADING OF MULTILAYERED CYLINDRICAL  
GEOMETRIES IN THERMAL CYCLING FROM 300 TO 1300 K

R. C. Hendricks and G. McDonald  
National Aeronautics and Space Administration  
Lewis Research Center  
Cleveland, OH 44135

R. L. Mullen  
Case Western Reserve University  
Cleveland, OH 44106

M. J. Braun, B. T. Chung, and J. Padovan  
University of Akron  
Akron, OH 44325

ABSTRACT

The principle of multiple material layering is well known as an effective method of reducing heat transfer; however, thermal gradients can impose significant mechanical loads and lead to delamination and subsequent component failure. An analysis is developed and experimental data are discussed for the thermomechanical effects of multilayered materials on a heat sink substrate of cylindrical geometry subject to thermal cycling. The geometry is heated in cross-flow by a high-velocity flame and cooled in crossflow by ambient-temperature air from a critical flow orifice. Each layer of material possesses a threshold beyond which small changes in temperature or mechanical loading greatly influence the life in thermal cycling of the layered materials. Comparisons are made between the thermomechanical loads predicted by various numerical codes for the linear case and by a simplified analytic model.

NOMENCLATURE

A	area
AR	aspect ratio
a,b	exponent, eq. (8)
Co	constant, eq. (8)
D	diameter
E	modulus of elasticity
F	temperature ratio function, eq. (2)
FE	finite element
h	heat transfer coefficient
k	thermal conductivity
L	axial length
M	Mach number
N	number of cycles
Pr	Prandtl number
q	heat flux
Re	Reynolds number
r	radial coordinate, rads
So	standard deviation
T	temperature
t	thickness

u	displacement
y	exponent, eq. (2)
z	axial coordinate
$\alpha$	thermal expansion coefficient
$\Delta$	differential
$\epsilon$	strain
$\dot{\epsilon}$	strain rate
$\epsilon_p$	plastic strain
$\theta$	circumferential coordinate
$\sigma$	stress
$\tau$	time

#### Subscripts:

cr	creep
h	heating
f	film
p	pulloff
q	heat flux
s	surface
rr	radial
zz	axial
zr	axial-radial (shear)
$\theta\theta$	circumferential
$\infty$	free stream, bulk
0	reference value
1,2	reference materials

#### Superscripts:

+	transient, eq. (19)
*	related to pull-off, eq. (19)

## INTRODUCTION

### Toward Higher Engine Efficiencies

Improved engine efficiency without a sacrifice in operating life is a major goal of the propulsion community. In 1981, U.S. airlines consumed a billion gallons of fuel; a one-point increase in efficiency could have resulted in a savings of some \$60 M (ref. 1). One method of achieving higher efficiencies is to increase the cycle operating temperature. To prolong operating life at these temperatures, components can be covered with multiple layers of plasma-sprayed materials.

### Plasma Sprayed Surfaces

The potential use of plasma-sprayed layered materials is promising, but not without difficulties and limitations. Previous experimental work (refs. 2-8) has shown that yttria-stabilized zirconia ( $ZrO_2-Y_2O_3$ ) ceramic coatings plasma sprayed onto a metal substrate fail after varying lengths of time when cyclically heated by exposure to high-temperature, high-heat-flux flames. The ability to predict the life of these layered materials is made difficult because several modes of failure or degradation exist, including spalling, erosion, corrosive attack, and corrosive oxidation of the bondcoat. The failure occurs principally in the ceramic at the bondcoat interface.

Although the mechanisms that control these failure modes are not well understood, when spalling or debonding occurs, the adverse effects include direct exposure of structural substrates to the high-temperature environment.

### Objectives

In many cases the heat transfer can be evaluated, but the coupled thermomechanical response of specimens in both the spacial coordinates and time is not known. One needs to investigate the effects of heating and cooling transients, time at temperature, and heat flux, coupled with elastic and inelastic material behavior.

In this paper we model the cyclic heating and cooling of a cylindrical, multilayered specimen alternately placed in high-velocity hot and cold gas streams, in crossflow. We want to address variations in thermal profiles and stresses due to modeling and computational codes by having researchers independently, but cooperatively, look at the same problem. Thus we look at the results from the thermal codes ADINAT, MARC, and SINDA and the stress codes ADINA, MARC, and FEATS.

## MODELING CONSIDERATIONS

### Thermocycling

It has been determined that thermal stresses in layered protective ceramic coatings are sensitive to the heating rates and that short heating cycles greatly decrease life in terms of total time at temperature (ref. 2). Furthermore a 0.076-cm-thick surface material failed immediately and a 0.038-cm-thick surface material failed some number of cycles later. Thus for our problem the heating and cooling boundary conditions will be related to short cycles, 3 to 5 minutes of heating, and 2 to 3 minutes of cooling. The thickness of the multilayered materials can be varied. For comparison, we start with a 0.038-cm thickness and thermocycle to an equilibrium temperature of 1311 K (1900° F).

### Limiting Life Temperature

In reference 6 the effects of heating rate and operating temperature were explored by varying the initial or startup fuel-air ratio (F/A). At a reduced (F/A), flat-plate specimens ran over  $1 \times 10^4$  cycles without failure, but at an elevated (F/A) such specimens ran less than 400 cycles to failure. Most importantly, the surface temperatures were 900 (1650) and 982° C (1800° F), respectively. The analysis showed a lower stress (20 percent) at 900° C, which did not explain the large change in cyclic life. This implies the existence of a threshold temperature for the model (i.e., above 900° C).

### Cycle Life and Adhesive/Cohesive Strength

In reference 7 a statistical study of 22 cylindrical rod specimens (exposed to high-heat-flux conditions) and 24 cylinder disk pulloff specimens (no exposure) was made in an effort to define a failure model and relative strengths. Four failure mechanisms (strain relief, heating rate, stress reversal, and ceramic voids) were cited. The data sets were better described by log-normal distributions. Such a distribution where the failure rate decreases as run cycles increase could be related to the threshold temperature, as stated in the preceding section. The data of reference 7 will be used in our calculations.

### Effects of Combustion Gases

In reference 8 tests with salts indicated that some would cause immediate coating failures (e.g., vanadium compounds), while others would take somewhat longer (e.g., magnesium compounds). The failure mechanism could be the interstitial condensation of salts in the ceramic along with oxidation of the bondcoat. In this analysis, we consider only clean gases.

### Substrate Precooling

In reference 9 the substrate temperature was systematically varied, and in reference 10 an optimum region 21 to 316° C was reported. This implies some residual stresses, but their magnitudes are unknown, so we will consider an initially stress-free coating.

### Plasma Arc Power

In reference 11 the use of plasma-spray arc power increased specimen life somewhat with increasing arc current (525 to 950 A). At least two effects are noted; the porosity of the coating decreases and the development of a microcrack network increases with increasing arc power (See also the motion picture supplement). In addition, a higher quench heat transfer coefficient due to increased impact velocity, substrate heatup, larger droplet mobility, and wetting characteristics upon impact are suspected to have an effect. We will not consider microstructure in our model directly; however, we will use the sample data sets of reference 7, which were sprayed at 650 A.

### Thermal Shock Effects

Crack propagation and arrest (thermal shock) are inherent to all these studies. Analysis and testing of SiO<sub>2</sub> and ZrO<sub>2</sub> fiber materials demonstrated high-temperature capabilities, but strengths are low and bonding techniques undeveloped (ref. 12).

Since no microstructure will be considered, the layers modeled depend only on bulk material properties. However, in this analysis we will consider only one type of coating, ZrO<sub>2</sub>-Y<sub>2</sub>O<sub>3</sub> (yttria-stabilized zirconia, or YSZ).

### Inelastic Behavior (Creep) - A Significant Factor

Some effects of high-temperature inelastic behavior are presented in reference 13, where a form for creep behavior is established. Furnace tests demonstrate creep effects for plasma-sprayed YSZ disk specimens and YSZ-Bond-Substrate bar specimens. These tests show that significant creep begins near 1000° C (see the section Limiting Life Temperature) and that the bondcoat (NiCrAlY) still retains sufficient strength to creep the YSZ at temperatures to 1177° C.

In all cases the experiments and analysis show a sensitivity to temperature and thermophysical properties. These results may be qualitatively summarized as:

1. That if the sample can withstand the thermal shock (remain within the elastic range), then creep and oxidation/corrosion must be considered.
2. At increased thermomechanical loading, failure can occur during cool-down or subsequent thermal shock phases where the additional strain due to creep causes a stress load beyond the capacity of the coating and it fails.

For the initial development of the numerical models, elastic behavior is considered; in the simplified model, creep is considered.

## Toward Ceramic Components

A monolithic ceramic turbine blade with cooling slots was proposed, and operated, during the World War II; see reference 14 for photographs. More recently, a similar concept was proposed in reference 15 using YSZ. Computational heat transfer and industrial applications of ceramic-sprayed components (turbine blades, seals, pistons, etc.) are explored in references 16 to 19. The details of predicting turbine blade temperatures and the narrow operating range (within  $\pm 30^\circ \text{C}$ ) along with the thermal profiles for the sprayed blades are provided in references 20 and 21. In reference 22 various heat transfer correlations for internal cooling of turbine blades are investigated, and recommendations and limitations for their use are presented.

Although the model can be applied to these more complex configurations, we will model a cylindrical geometry.

## HEAT TRANSFER ANALYSIS

### Heat Transfer Coefficients

Accurate information for the convective heat transfer coefficient to and from cylinders exposed in a stream of air is essential for evaluating the cylinder's surface temperature and heat flux to and from this surface. In addition to the convective path there is a radiative path, but the latter becomes important only at relatively low Reynolds numbers ( $1 \times 10^2$  to  $1 \times 10^3$ ) or when rather large temperature differences are acting between the cylinder's surface and the environment.

From a literature study (refs. 23-27) we have decided to adopt separate heat transfer coefficients for the heating and cooling of the cylinder. The correlations are valid for cylinders with smooth surfaces, and will be used even though the plasma-sprayed finish of the ceramic cannot be considered smooth.

Heating. A relationship put forward by Churchill and Brier (ref. 23) which correlates the experimental data (refs. 27-29) with the physical properties evaluated at  $T_\infty$  was adopted.

Although the test cylinder temperature varies in both the axial and circumferential coordinates, the variations are small relative to the radial gradient. Thus, integrating over  $\theta$ , the average value of the Reynolds number exponent becomes  $n = 1/2$ ; the model is now assumed to be axisymmetric.

$$\text{Nu}_\infty = \frac{hD}{k_\infty} = 0.6 \text{Re}_\infty^{1/2} \text{Pr}_\infty^{1/3} \left( \frac{T_\infty}{T_s} \right)^{0.12} \quad (1)$$

According to Morgan (ref. 27) when the intensity of the turbulence is taken into consideration for  $\text{Re} > 1 \times 10^4$ , the heat transfer coefficient can increase by 18 to 37 percent depending on the intensity. It is apparent that neither reference 23 or King (ref. 29) nor Hiplert (ref. 30) have included the effects of the turbulence intensity in their correlations, and this also represents a limitation of our analysis.

Cooling. For the cooling part of the cycle, most of the experimental data available have been fitted to a family of equations over a range of Reynolds numbers. Fand and Keswani (ref. 24) developed correlation for a Reynolds number range between  $1 \times 10^{-2}$  and  $2 \times 10^5$ . The expression they proposed is

$$Nu_f = \left( 0.184 + 0.324 Re_f^{1/2} + 0.291 Re_f^{0.5+y} \right) F \quad (2)$$

$$F = \left( \frac{T_f}{T_\infty} \right)^{0.17}$$

where

$$y = -0.253 + 0.0407 Re_f^{0.168}$$

$$T_f = \frac{(T_\infty + T_s)}{2}$$

$T_f$  and  $T_\infty$  being the absolute film and ambient temperatures, respectively. Since the properties are evaluated at the film temperature, the heat transfer coefficient is no longer represented by a simple algebraic function in terms  $T_s$ .

The third term inside the brackets of equation (2) represents the heat transfer on the front and rear portions of the cylinder; and equation (2) calculates an averaged heat transfer coefficient for the whole cylinder.

#### NUMERICAL THERMAL MODELING CODES

In general, the experimental applications will involve nonsymmetric geometries with temperature gradients in all three coordinates ( $r, \theta, z$ ) due to external and internal flows. Herein we will treat the body as a uniformly heated cylindrical heat sink.

#### ADINAT (ref. 30).

A 0.038-cm-thick ceramic coating, yttrium-stabilized zirconia (YSZ), is plasma sprayed over a 0.013-cm-thick nickel-chromium-aluminum-yttria (NiCrAlY) bondcoat. The stainless substrate\* is 1.30 cm in diameter.\*\*

Figure 1(a) shows the finite element model of the system of 18 elements and 93 nodes. Although the 4-node element could be used, the 8-node element was chosen in order to obtain better results for the stress calculation. A refined grid with 333 nodes and 66 elements produced nearly the same temperature distribution.

Heating and Cooling Cycles. Figure 2 presents temperature distributions during the heating and cooling periods.

---

\*The substrate material used in the tests (e.g., refs. 2, 22) Rene 41 or Inconel are classified as super alloys. Upon direct exposure to the 0.3 Mach burner flame, these substrates corrode slowly; 304-stainless steel corrodes rapidly, has a higher thermal expansion coefficient and would be a poor choice of substrate material; the coating is, however, very protective and 304 is used in this study for simplicity and as a parametric term.

\*\*1.27 cm diameter was used in the MARC code and both 1.27 and 1.3 cm were used in SINDA-FEATS with little change in the results.

The hot gas temperature is 1311 K during the first 5 minutes, and the cold gas temperature is 298 K in the next 3 minutes. The label "ZrO<sub>2</sub>-interface" represents the ceramic-bondcoat interface. Since the bondcoat-substrate interface temperature difference is only about 5 K, it is not shown. In the calculations, all thermal properties except density are considered to be temperature dependent. Those properties, shown in table I, are the input to ADINAT. The program picks up the appropriate value by linear interpolation.

For heating, the heat transfer coefficient proposed by Church and Brier (ref. 23, eq. (1)) was used. Since all properties are evaluated at the bulk stream temperature of the hot gas, equation (1) can be easily converted to a simple formula with the aid of gas tables and known burner Mach number (0.3); for our problem this becomes

$$h = \frac{916.6}{T_s^{0.12}} \frac{W}{m^2-K} \quad (3)$$

This formula is also fed into ADINAT through input.

As for the cooling process, the correlation by Fand and Keswani (ref. 24, eq. (2)) has been adopted. All fluid properties are now evaluated at the film temperature, and the heat transfer coefficient is a more complex function of surface temperature. A table of  $h$  vs  $T_s$  was constructed and was also fed into ADINAT through input.

Coupling of the Heat Transfer Coefficient. To demonstrate the significance of a variable heat transfer coefficient, we repeated the same problem of heating for the first 14 seconds by using a uniform heat transfer coefficient,  $h = 511 \text{ W/m}^2\text{-K}$  ( $90 \text{ B/hr-ft}^2\text{-F}$ ). The dashed lines in figure 3 represent the numerical solutions for this case. As can be seen, the difference between the solid and dashed lines continues to grow as time increases, until equilibrium is reached. Since the temperature of the solid varies over such a wide range, and in turn gives rise to thermal stress fluctuations, the temperature-dependent heat transfer coefficient and other thermal properties should not be neglected.

MARC (ref. 31).

For the axisymmetric heat transfer analysis, internal to MARC, the geometric configuration discussed in connection with ADINAT was adopted. This method, like ADINAT, is a finite element method.

Figure 1(b) shows the finite element model consisting of 72 elements and 293 nodes. The 8-node isoparametric, axisymmetric element was used to obtain both thermal and stress calculations. The system simulated a set of 4 stacked disks (elements) when combined with a symmetry condition along the center plane; this approximates a cylinder of length  $2L$ .

Although the thermal analysis is essentially one-dimensional, the use of several elements in the axial direction allows coupling of the thermal and stress analyses without the use of a mapping function from one mesh to another.

In the section Temperature profiles, we cite the use of symmetry and free end conditions on  $z$  to simulate a short cylinder and fixed end conditions at both  $z = 0$  and  $z = 2L$  to simulate the infinite cylinder. For either case the temperature does not vary in the axial ( $z$ ) direction.

Thermal boundary condition subroutine. A subroutine was written to describe the convective (radiative) boundary conditions. These conditions

have been described above and are given by equations (1) and (2) for heating and cooling, respectively. Either the Dirichlet or Neumann conditions can be calculated in such a subroutine as a normal part of the MARC thermal analysis and can be easily adapted to handle more complex formulations such as may be required for axial and circumferential variations in surface temperature.

Temperature profiles. Graphs of the surface, the interfaces between the ceramic, bondcoat, and substrate and the centerline for heating and cooling, are similar to those shown as figure 2 and will not be repeated here. The difference here is that we have elected to use a superalloy (ref. 17) to represent the substrate. Since the superalloy has a lower thermal conductivity than type 304 stainless steel, the relative interface temperatures are about 50 K higher for the transient.

SINDA (refs. 32,33).

In contrast to the other codes, which are finite element, SINDA is a finite difference code. Again, the geometry adopted is that described in the section Heat Transfer Coefficients. The properties are now represented as lumped values. To make the temperature profiles available to the mechanical code FEATS, the average element temperature must be interpolated to provide values at each node. Across each interface the average thermal conduction is represented by the inverse sum of the conductivities.

We used both a 40-element, 82-node model and a 105-element, 212-node model and achieved about the same results with both. The models, shown in figure 1(c), had 10 elements in the ceramic, 10 in the bondcoat, and 10 in the first 0.038 cm (0.015 in.) of the substrate. The remainder of the elements, either 10 or 75, uniformly partitioned the remainder of the substrate. It was felt that such a division would capture the extreme gradients in the ceramic, especially at the bondcoat-ceramic interface.

### Comparisons

Although three different numerical techniques, average and variable thermophysical properties, and heat transfer coefficients were explored, the profiles were within 100 K. In this analysis, such a variation is small (10 percent) when compared with the absolute level and range of parameters considered. These results are also in reasonable agreement with the experimental temperatures measured at the interface (ref. 2).

## STRESS ANALYSIS

The coupled heat transfer and stress analysis, termed thermomechanical analysis, enables one to combine the effects of mechanical loads imposed by surface tractions (e.g., skin friction and pressure drop) and body force effects (e.g., rotation, takeoff, and maneuvering) with those thermal loads imposed by changes in internal energy and volume. (It is hoped that the composition remains fixed.) Although these effects must be considered in application herein, we will consider a traction and body force-free axisymmetric geometry.

### Simplified Model

Two-layer model with creep. Consider a two-material, cylindrical, heat sink model of multilayered ceramic with a stress-time history as illustrated

in figure 4. To determine the stress at the interface, including the effects of creep, the following equations must be satisfied:

$$\text{Compatibility } \epsilon_1 - \epsilon_2 = 0 \quad (4)$$

$$\text{Equilibrium } \sigma_1 A_1 + \sigma_2 A_2 = 0 \quad (5)$$

$$\text{Constitutive } \epsilon = \alpha \Delta T + \frac{\sigma}{E} + \int_0^{\tau_h} \dot{\epsilon}_{cr} d\tau + \epsilon_p \quad (6)$$

For the simplified model (fig. 4(b)) the stress becomes

$$\sigma = \sigma_2 = - \left[ \frac{E_2}{1 + \left( \frac{E_2 A_2}{E_1 A_1} \right)} \right] \left[ \alpha_2 \Delta T_2 - \alpha_1 \Delta T_1 + \int_0^{\tau_h} (\dot{\epsilon}_{cr_2} - \dot{\epsilon}_{cr_1}) d\tau + \epsilon_p \right] \quad (7)$$

Further assume that the system is isothermal (i.e.,  $\Delta T_1 = \Delta T_2 = \Delta T$ ) and

$$\dot{\epsilon}_{cr} = C \sigma^a \tau^b e^{-Q/RT} \quad (8)$$

Homogeneous body approximation. Let material 2 be the YSZ ceramic and material 1 the substrate, say Inconel. With the geometric and material constants given in the next section,  $A_2/A_1 = 4t/d = 0.12$ ,  $A_2 E_2/A_1 E_1 = 0.07$  and assuming  $\dot{\epsilon}_{cr} = \dot{\epsilon}_{cr_2} \gg \dot{\epsilon}_{cr_1}$ , equation (7) may be approximated as

$$\epsilon = \frac{\sigma}{E} = -\Delta \alpha \Delta T - \int_0^{\tau_h} \dot{\epsilon}_{cr} d\tau - \epsilon_p \quad (9)$$

The ceramic creep rate may be expressed as (ref. 13).

$$\dot{\epsilon}_{cr} = 2.39 \times 10^{-3} \tau^{-0.45} \sigma e^{-1230/(T-T_{ref})} \quad (10)$$

where the units of  $\tau$ ,  $\sigma$ , and  $(T - T_{ref})$  are minutes, MPa, and K respectively. Differentiating, equation (9) becomes

$$\dot{\sigma} = -A_0 \sigma \tau^{-0.45} \quad (11)$$

where

$$A_0 = 2.39 \times 10^{-3} E e^{-1230/(T-T_{ref})} \quad (12)$$

Solving, equation (11) becomes

$$\epsilon = \frac{\sigma}{E} = \epsilon_0 e^{-1.82A_0\tau^{0.55}} \quad (13)$$

From the initial conditions it is known that

$$\epsilon_0 = -\Delta\alpha\Delta T - \epsilon_p \quad (14)$$

and subtracting the initial strain equation (12) becomes

$$\epsilon = \epsilon_0 \left( 1 - e^{-1.82A_0\tau^{0.55}} \right) \quad (15)$$

Effect of N cycles. For N heating cycles, each of time  $\tau_h$  minutes, we may approximate the total time of creep as  $\tau = \sum \tau_i \sim \tau_h N$ . If the limiting strain is governed by a relation to the pull off strength of the ceramic (i.e., the adhesive-cohesive strength), the developed strain can be related as

$$\epsilon = \frac{\sigma_p r}{E_0 t} \quad (16)$$

Estimates for interface stress. The following numerical values are used to estimate the stresses at the bondcoat-ceramic interface:

$$\begin{aligned} T_S - T_0 &= 1000 \text{ K (1800}^\circ \text{ F)} \\ T_S &= 1311 \text{ K (1900}^\circ \text{ F)} \\ \Delta\alpha &= 7.2 \times 10^{-6} \text{ (4} \times 10^{-6} \text{)} \\ E &= 1.38 \times 10^4 \text{ MPa (2} \times 10^6 \text{ psi)} \\ E_0 &= 4.8 \times 10^4 \text{ MPa (7} \times 10^6 \text{ psi)} \\ r &= 0.66 \text{ cm (0.26 in.)} \\ t &= 0.038 \text{ cm (0.015 in.)} \\ \sigma_p &= \bar{\sigma}_p \pm S_0 \text{ (9} \pm 4.5 \text{ MPa) (1300} \pm 650 \text{ psi)} \\ &\quad \text{for 24-specimen set (ref. 7)} \\ \sigma_p &= \bar{\sigma}_p \pm S_0 \\ &= 6.2 \pm \sigma_p/2 \text{ MPa (900} \pm \sigma_p/2 \text{ psi)} \\ &\quad \text{for 4-specimen set (ref. 3)} \end{aligned}$$

Before we determine any values, we can solve for  $\tau = N\tau_h$

$$\tau = \left[ \frac{-\ln \left( 1 - \frac{\epsilon}{\epsilon_0} \right)}{1.82A_0} \right]^{1.82} \quad (17)$$

Assume that  $\epsilon_p \sim 0.05$  percent. Solving equation (17) gives  $\tau = 2.98 \times 10^3$  minutes, and for N identical cycles each of  $\tau_h = 3$  minutes at temperature T,  $N = 990$ .

The sensitivity of the results to variations in temperature and coating pulloff strength is illustrated in table II.

Thermal transient effects. During the transient, the radial temperature gradient is strong and must be included. For constant heat flux the strain becomes (ref. 2)

$$\epsilon_q = \frac{\sigma}{E} = \frac{\Delta\alpha qt}{2k(1-\nu)} \quad (18)$$

which is effective primarily in the initial phases of the heating and cooling portions of the cycle. During the latter part of either cycle, as equilibrium is approached, the isothermal case would apply. (This would not be the case for an internally cooled specimen where a radial gradient would always be present.) Thus one can consider the heat flux to decrease. The allowable radial stress is

$$\sigma_{rr}^+ = \sigma_{rr}^* - \frac{E \Delta\alpha qt^2}{2k(1-\nu)r} \quad (19)$$

For  $q = 550 \text{ kW/m}^2$ ,  $k = 0.069 \text{ cm-kW/m}^2\text{-K}$ ,  $\nu = 0.25$ ,  $E = 4.8 \times 10^4 \text{ MPa}$ , and  $\Delta\alpha = 6 \times 10^{-6}/\text{K}$ , the effective radial stress becomes 3.36 MPa and so the allowable pulloff stress, which we assume to be related to  $\sigma_{rr}$ , decreases from 9 MPa (1300 psi) to 5.64 MPa (820 psi). This changes  $\epsilon$  to  $\epsilon^+$  as follows,

$$\epsilon^+ = \frac{\sigma_{rr}^+ r}{E_0 t} \quad (20)$$

The effects of the transient stresses in addition to the stresses created by creep, for variations in temperature and allowable stress, are illustrated in table III.

#### Numerical Stress Modeling Codes

In this section we present figures which define the thermomechanical response of a multilayered cylinder. For each numerical model and code we include a brief writeup relating to element type, mesh refinement, boundary conditions (mechanical/thermal), and material properties and discuss some of the results.

ADINA (mechanical FE model) (ref. 34). The element type employed was the small deformation, linear, thermoelastic material model which accounts for temperature-dependent data. The element is eight-node, two dimensional, isoparametric, and axisymmetric and is illustrated as figure 5(a). The axial z coordinate was chosen at 0.05 cm (0.020 in.) to maintain an acceptable aspect ratio (AR), thereby minimizing unrealistic distortion of the elements.

The mesh was refined to determine the sensitivity of the model to variations in node spacing. The coarse- and fine-grid models are illustrated in figure 1(a). The coarse mesh consisted of 18 elements, 4 in the ceramic, 1 for the bondcoat, and 14 in the substrate. The refined mesh consisted of 66 elements: 8 in the ceramic, 4 in the bondcoat, and 54 in the substrate for a total of 333 nodes and 666 degrees of freedom.

The thermal boundary conditions discussed in the section HEAT TRANSFER ANALYSIS are enforced. The mechanical conditions are illustrated in figure 5(a).\*\*\* In all cases the surfaces are traction free with  $\sigma_{rr}$  and

---

\*\*\*For the experimental case, there is always a temperature and a pressure distribution as well as a mechanical reaction to loadings and most likely flutter. While these loads are usually considered small, they will contribute to coating failures.

$\sigma_{rz} = 0$  at  $r = R_0$  and displacements at  $r = 0$ ,  $u_r = 0$  because of symmetry and at least a node where  $u_z = 0$ .

Material properties and geometry: The temperature-dependent mechanical properties of the ceramic, bondcoat, and substrate used in this model are given in table I. It should be noted that the effective composition of the ceramic can be altered or graded, thereby adding other layers. Likewise can the bondcoat be altered and strain isolation provided. The substrate can also be graded. Thus multilayers can be used, but we broadly classify these as ceramic, bondcoat, and substrate.

Some tentative results and conclusions: The calculated axial, radial, and circumferential stresses generated in a ceramic-coated cylinder are given in figure 6. These stresses result from the applied thermal and mechanical loadings described in the preceding sections. In this case, we have confined our attention to the material interfaces (figures 1 and 6), which represent maximum changes in stresses ('kinks' in the strain locus), and to the first 15 seconds of the heating cycle to minimize the information presented.

(1) Runs involving both coarse and fine meshes (18 and 66 elements) yield essentially equivalent results, but proper selection of node spacing is paramount.

(2) Initial transient mechanical results, heating, and cooling are highly sensitive to the description of thermal profiles and mechanical boundary conditions.

(3) Severe discontinuities in the ceramic, bond, and substrate properties yield adverse stress gradients; one needs to explore more compatible choices of material properties and geometries to define 'best' material-geometry pairing. It is hoped that materials science will generate requisite material properties combining good life (fatigue, fracture, etc.) (refs. 35-37).

(4) Although ceramic properties have a profound effect on the thermal profile, it has little mechanical influence on stresses in the substrate. It appears that ceramic stresses (for times  $> 5$  sec) are 'going along for the ride' generated by substrate expansion. This would be especially true for a thin ceramic layer.

MARC (mechanical/thermal FE model) (ref. 31). In this model (figs. 1(b) and 5(b)) we have extended the planar axisymmetric model to include an axial portion of the cylinder. We have considered two types of boundary conditions, fixed and free, realizing that the heated section of the experimental cylinder, modeled herein, satisfies neither; however, the results will be bounded by these two classic boundary conditions.

For the fixed end conditions, no axial displacement at  $z = 0$  or  $z = 2L$  (free in  $r$ ), the model simulates the infinite cylinder. For the free end conditions, fixed at  $z = 0$  (free in  $r$ ) with no constraints on displacement at  $z = 2L$ , the model simulates a short cylinder of length  $4L$  symmetric about the plane  $z = 0$ . Some of these results are presented as figure 7 for fixed end planes and figures 8(a) and (b) for free end planes for the thermal loadings discussed in the section NUMERICAL THERMAL MODELING CODES.

Figure 7 shows that during the heating phase, the radial stress changes from tensile, initially, to compressive near equilibrium. The axial stresses are compressive and large. The circumferential stresses are at first compressive but quickly change to large tensile values. (Recall that this is an elastic analysis without failures.) During the cooling phase the stress magnitudes decrease, but not as dramatically as with heating.

Figure 9 illustrates how the radial stresses change with heating and cooling at four locations near the bondcoat-ceramic interface. As can be

seen, the maximum tensile stress moves radially toward the surface and can be thought of as a thermal-driven stress wave. Failure of a ceramic under these conditions would be expected to move from the interface to slightly into the ceramic. For thicker ceramics the failure plane should move even further toward the surface.

Figure 10 illustrates the 'bending stress' applied to the now barrel-shaped model. The inside elements (fig. 1(b)) represent the average of stresses over that element, so the actual values at the nodal points would be higher at  $z = 0$  and lower at  $z = L$ . The dramatic shift in the stresses from tensile to compressive results from the short-cylinder assumption and the applied thermal load (see the section NUMERICAL THERMAL MODELING CODES). The peak stresses occur within the ceramic, rather than at the interface. Experimentally, most failures appear to occur near the bondcoat-ceramic interface. If the model were homogeneous, subsurface cracking within the ceramic could be the dominant mechanism (refs. 39 and 40).

To determine some effects of finite element aspect ratio (AR), the element length was increased to unity. For the fixed constraint case the results do not differ to any significant degree.

FEATS (ref. 39). For this code the geometric conditions are the same as in the thermal modeling section, (figs. 1(c) and 6(c)), and the materials used were both superalloy and the 304 stainless steel. The code was run with fixed and free boundary constraints where the aspect ratio was kept  $0.5 < AR < 3$ , i.e.,  $\Delta z = 0.0025$  cm (0.001 in.). These constraints should bound the calculated stress for the experimental cylinder - if it remains elastic. In addition, the aspect ratio was made very large,  $40 < AR < 2000$ , i.e.,  $z = 2.54$  cm (1 in.). This tends to artificially stiffen the substrate yet enable the ceramic and interfaces to respond to large temperature gradients. It also artificially places the end constraint somewhere between fixed and free. Although the procedure is certainly questionable, the results correctly approach those theoretically predicted for homogeneous cylinders (ref. 40).

The temperature profiles were generated by SINDA using the thermal loading discussed in the section NUMERICAL THERMAL MODELING CODES. The numerical stress values were generated by FEATS. As can be seen, the radial stresses  $\sigma_{rr}$  are nearly the same for all three constraints, while the circumferential stresses  $\sigma_{\theta\theta}$  appear bounded by the free and fixed end constraint values. The axial stresses  $\sigma_{zz}$  follow these same trends. An exception occurs at the interface, where the fixed case stresses are large and compressive and the artificial case stresses are tensile.

In general, there is a much larger variation in the stress profiles predicted by ADINA, MARC, and FEATS than in the predicted thermal profiles, primarily because stresses are more sensitive to modeling methods than is the thermal analysis.

## SUMMARY

Various levels of sophistication in both the modeling and the codes have been considered. The modeling ranged from one-dimensional constant properties and first-order difference schemes with constant heat transfer coefficients to temperature-dependent heat transfer and material properties used with an eight-node (serendipity) finite element method. Five numerical codes were involved in producing three sets of thermomechanical behaviors: ADINAT-ADINA, MARC, and SINDA-FEATS. The results of these numerical codes and a simplified analysis are as follows.

1. For the heating and cooling of a multilayered cylindrical heat sink specimen, it is necessary to include temperature-dependent fluid and material properties and coupling of the heat transfer from the hot gas stream to the specimen.

2. Large thermal gradients, such as occur in multilayer-coated specimens, effect large thermoelastic strains, which for the elastic case give rise to high component stresses.

3. During the heating or cooling transient, large thermal gradients exist in the skin of the coating and enhance the probability of failure through crack propagation.

4. At steady operating temperatures, a simplified analysis indicates that inelastic behavior, creep, could play a significant role in specimen coating failure. It is suggested that the analysis be verified experimentally and through the use of numerical modeling of the multilayered-coated specimen.

5. The temperature predicted using one-dimensional finite elements and finite differences has a variation of about 60 K. At this time, such variations are thought to be the result of thermophysical properties and modeling procedures. It is also possible that there may be some variations due to solution techniques.

6. Coating failures usually occur at the ceramic-bondcoat interface. The calculated stresses at this interface, amplified by differences in thermal gradients, possess similar trends but the magnitudes differ. In general the elastic radial stresses are significantly less than the adhesive/cohesive strength (at room temperature); however, consideration of inelastic behavior may enhance the calculated radial stresses. These problems are yet to be resolved.

7. A major difficulty lies in characterizing problems which are neither plane strain nor plane stress. The desired result appears bounded between those for the fixed and free constrained disk-shaped surfaces of the model. An artificial constraint seems to provide results between these classic constraints but has not been explored in any detail. In general the application to the thermal problem is in violation of the field equations; nevertheless it is used.

8. The long- and short-cylinder behavior implies that the geometry either expands uniformly in the radial direction or it tends to 'barrel' at the plane of symmetry. Such behavior is characteristic of bending under thermal loads, but neither situation represents the finite cylinder. The next phase should look at the finite cylinder including axial and perhaps circumferential temperature gradients.

## REFERENCES

1. Haggerty, J. J., "Spinoff 1982," NASA TM-84826, Apr. 1982, National Aeronautics and Space Administration, Washington, D.C.
2. McDonald, G. and Hendricks, R. C., "Effect of Thermal Cycling on  $ZrO_2$ - $Y_2O_3$  Thermal Barrier Coatings," Thin Solid Films, Vol. 73, 1980, pp. 491-496.
3. Levine, S. R., "Adhesive/Cohesive Strength of a  $ZrO_{2.1-2}$  w/o  $Y_2O_3$ /NiCrAlY Thermal Barrier Coating," NASA TM-73792, 1978, National Aeronautics and Space Administration, Cleveland, OH.
4. Anderson, C. A., Bratton, R. J., Lau, S. K., Lee, S. Y., Allen, J., Munsen, K. E., and Rieke, K. L., "Advanced Ceramic Coating Development for Industrial/Utility Gas Turbines," NASA DEN3-110, Jan. 1981, National Aeronautics and Space Administration, Cleveland, OH.

5. Bill, R. C., "Creep Evaluation of Plasma Spray ZrO<sub>2</sub> Materials," To Be Published NASA CR.
6. Hendricks, R. C., McDonald, G. and Poolos, N. P., "Prolonging Thermal Barrier Coated Specimen Life by Thermal Cycle Management," NASA TM-81742, 1981, National Aeronautics and Space Administration, Cleveland, OH.
7. Hendricks, R. C. and McDonald, G., "Assessment of Variations in Thermal Cycle Life Data of Thermal Barrier Coated Rods," Thin Solid Films, Vol. 74, 1981, pp.
8. Miller, R. A., "Analysis of the Response of a Thermal Barrier Coating to Sodium and Vanadium Doped Combustion Gases," DOE/NASA/2593-79/7, NASA TM-79205, 1979, National Aeronautics and Space Administration, Cleveland, OH.
9. Sumner, I. E. and Ruckle, D. L., "Development of Improved-Durability Plasma Sprayed Ceramic Coatings for Gas Turbine Engines," AIAA Paper 80-1193, June 1980, American Institute of Astronautics and Aeronautics.
10. Cassenti, B. N., Brickley, A. M. and Sinko, G. C., "Thermal and Stress Analysis of Thermal Barrier Coatings," AIAA Paper 81-1482, July 1981, American Institute of Astronautics and Aeronautics.
11. Hendricks, R. C. and McDonald, G., "Effects of Arc Current on the Life in Burner Rig Thermal Cycling of Plasma Sprayed ZrO<sub>2</sub>-Y<sub>2</sub>O<sub>3</sub>," Presented at the 6th Conference on Composites, Cocoa Beach, Fla., Jan. 17-21, 1982, American Ceramic Society.
12. Hendricks, R. C. and McDonald, G., "Use of Fiber Like Materials to Augment the Cycle Life of Thick Thermoprotective Seal Coatings," Presented at the International Conference on Metallurgical Coatings and Process Technologies, San Diego, CA, Apr. 4-9, 1982, American Vacuum Society.
13. Hendricks, R. C., McDonald, G., and Bill, R. C., "Some Inelastic Effects of Thermal Cycling on ZrO<sub>2</sub>-Y<sub>2</sub>O<sub>3</sub> Thermoprotective Materials," presented at the 84th Annual Meeting and Exposition of the American Ceramic Society, Cincinnati, OH, May 1982.
14. Hendricks, R. C. and McDonald, G., "Some Thermal Stress Problems in Porcelain Enamel Coated Rods," Proceedings of the Porcelain Enamel Institute, Vol. 42, American Ceramic Society, 1980, pp. 178-183.
15. Stepka, F. S. and Ludwig, L. P., "Composite Wall Concept for High Temperature Turbine Shrouds: Heat Transfer Analysis," NASA TM-81539, 1980, National Aeronautics and Space Administration, Cleveland, OH.
16. Liebert, C. H. and Stepka, F. S., "Industry Tests of NASA Ceramic Thermal Barrier Coating," NASA TP-1425, June 1979, National Aeronautics and Space Administration, Cleveland, OH.
17. Sinko, G. S., Cassenti, B. N. and Brickley, A. M., "JT9D Thermal Barrier Coating Analysis Informal Report," PWA-55155-135, Sept. 1980, Pratt and Whitney Aircraft Group.
18. Bill, R. C., Wisander, D. W., and Brewe, D. E., "Preliminary Study of Methods for Providing Thermal Shock Resistance to Plasma-Sprayed Ceramic Gas-Path Seals," NASA TP-1561, May 1980, National Aeronautics and Space Administration, Cleveland, OH.
19. Hudson, M. S., Janovicz, M. A. and Rockwood, F. A., "Ceramic Applications in Turbine Engines," EDR-10156, May 1980, Detroit Diesel Allison, Indianapolis, Ind. (NASA CR-159865).
20. Gladden, H. J., "Similarity Tests of Turbine Vanes-Effects of Ceramic Thermal Barrier Coatings," ASME 80-HT-24, July 1980, American Society of Mechanical Engineers.
21. Stepka, F. S., "Uncertainties in Predicting Turbine Blade Metal Temperatures," ASME 80-HT-25, July 1980, American Society of Mechanical Engineers.

22. Yeh, F. C. and Stepka, F. S., "Review and Status of Heat Transfer Technology for Internal Passages of Air Cooled Turbine Blades," E-1373, 1982.
23. Churchill, S. W. and Brier, J. C., "Convective Heat Transfer from a Gas Stream at High Temperatures to a Circular Cylinder Normal to the Flow," Chemical Engineering Progress Symposium Series, Vol. 51, No. 17, 1955, pp. 57-66.
24. Fand, R. M. and Keswani, K. K., "A Continuous Correlation Equation for Heat Transfer from Cylinders to Air in Crossflow for Reynolds Numbers from  $1.E-2$  to  $2.E5$ ," International Journal of Heat and Mass Transfer, Vol. 15, Mar. 1972, pp. 559-562.
25. Churchill, S. W. and Bernstein, M., "A Correlating Equation for Forced Convection from Gases and Liquids to a Circular Cylinder in Crossflow," Journal of Heat Transfer, Vol. 99, No. 2, May 1977, pp. 300-306.
26. Krall, K. M. and Eckert, E. R. G., "Local Heat Transfer Around a Cylinder at Low Reynolds Number," Journal of Heat Transfer, Vol. 95, No. 2, May 1973, pp. 273-275.
27. Morgan, V. T., "The Overall Convective Heat Transfer from Smooth Circular Cylinders," Advances in Heat Transfer, Vol. 11, Academic Press, New York, 1975, pp. 199-264.
28. Kennelly, A. E. and Sanborn, H. S., "The Influence of Atmospheric Pressure upon the Forced Thermal Convection from Small Electrically Heated Platinum Wires," Proceedings of the American Philosophical Society, Vol. 53, 1914, p. 55-77.
29. King, L. V., "On the Convection of Heat from Small Cylinders in a Stream of Fluid," Philosophical Transactions of the Royal Society (London), Vol. 214, 1914, pp. 373-432.
30. Bathe, K. J., "ADINA - A Finite Element for Automatic Dynamics Incremental Non-Linear Analysis of Temperature," Rept. 82448-5, 1978, M.I.T., Cambridge, MA.
31. MARC-IBM-REV. J.2-1, MARC Analysis Research Corp., Palo Alto, CA.
32. Smith, J. P., "Systems Improved Numerical Differencing Analyzer (SINDA)," TRW-14690-H001-RO-00, Apr. 1971, TRW Systems Group, Redondo Beach, CA. (NASA CR-134271).
33. Cowgill, G. and Manos, P., "Private Communications.
34. Bathe, K. J. "ADINAT - A Finite Element for Automatic Dynamics Incremental Non-Linear Analysis," Rept. 82448-1, 1975, M.I.T., Cambridge, MA.
35. Levine, S. R., "High Temperature Surface Protection," NASA TM-73877, 1978, National Aeronautics and Space Administration, Cleveland, OH.
36. Stecura, S., "Effects of Compositional Changes on the Performance of a Thermal Barrier Coating System," NASA TM-78976, Aug. 1978, National Aeronautics and Space Administration, Cleveland, OH.
37. Stecura, S., "Effects of Yttrium, Aluminum, and Chromium Concentrations in Bond Coatings on the Performance of Zirconia-Yttria Thermal Barriers," NASA TM-79206, July 1979, National Aeronautics and Space Administration, Cleveland, OH.
38. Swanson, J. A., "FEATS - A Computer Program for the Finite Element Thermal Stress Analysis of Plane or Axisymmetric Solids," WANL-TME-1888, Dec. 1968, Westinghouse Electric Corp., Pittsburgh, PA.
39. Ainsworth, J. H. and Herron, R. H., "Thermal Shock Damage Resistance of Refractories," American Ceramic Society Bulletin, Vol. 53, No. 7, July 1974, pp. 533-538.
40. Boley, B. A. and Weiner, J. H., Theory of Thermal Stresses, John Wiley and Sons, New York, 1960.

TABLE I. - REPRESENTATIVE THERMOPHYSICAL PROPERTIES

Property	Temperature, K	Bondcoat (NiCrAlY)	Ceramic coat (ZrO <sub>2</sub> -Y <sub>2</sub> O <sub>3</sub> )	Substrate 304-stainless
Thermal conductivity, W/cm-K	283	0.05769	0.00721	0.13848
	1352	0.16589	0.02164	0.3346
	1770	0.2082	0.02728	0.41129
Density, kg/cm <sup>3</sup>	All	0.00698	0.00567	0.00782
Specific heat, J/kg-K	283	490.5	490.5	406.1
	1367	711.8	670	544.3
	1770	794	736.7	595.6
Modulus of elasticity, MPa	283	12.4x10 <sup>4</sup>	4.48x10 <sup>4</sup>	19.58x10 <sup>4</sup>
	811	11.72	3.21	15.65
	1144	4.42	2.41	11.65
	1367	<sup>a</sup> 0.0	1.88	8.55
Thermal expansion, 1/K	283	12.6x10 <sup>-6</sup>	7.86x10 <sup>-6</sup>	17.1x10 <sup>-6</sup>
	811	13.86	10.08	18.59
	1144	16.2	11.52	19.53
	1367	18	12.24	20.16

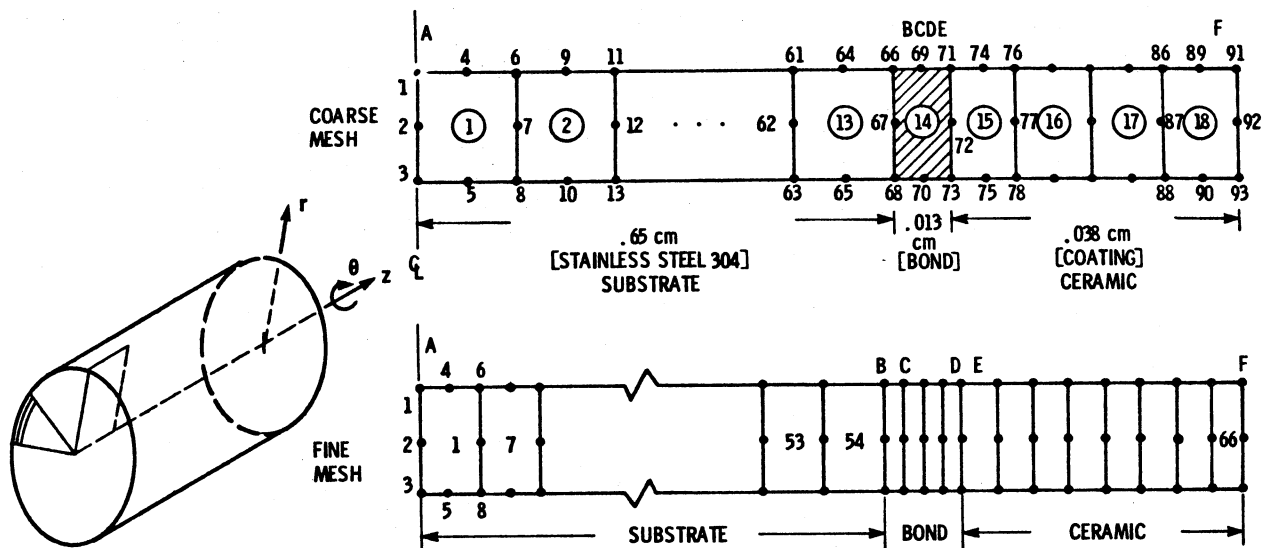
(<sup>a</sup>Probably <1x10<sup>5</sup>).

TABLE II. - ESTIMATE FOR NUMBER OF CYCLES TO FAILURE FOR VARIATIONS IN TEMPERATURE AND ALLOWABLE STRESS AT TWO DIFFERENT HEATING TIMES

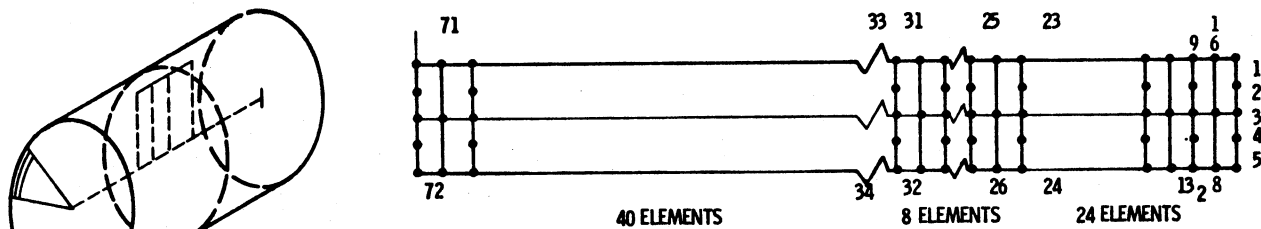
Allowable stress	Number of 3-minute cycles to failure			Number of 57-minute cycles to failure		
	Calculated at inter-face temperature-		Experimental 24-specimen data set (ref. 7)	Calculated at inter-face temperature-		Experimental 4-specimen data set (ref. 2)
	1283°K (1850° F)	1311°K (1900° F)		1283°K (1850° F)	1311°K (1900° F)	
$\sigma_p = \bar{\sigma}_p - S_0$	$1.3 \times 10^4$	200	810	315	5	50
$\sigma_p = \bar{\sigma}_p$	$6 \times 10^4$	990	1330	1350	22	180
$\sigma_p = \bar{\sigma}_p + S_0$	$2 \times 10^5$	3340	1870	3585	58	250

TABLE III. - ESTIMATE FOR NUMBER OF CYCLES TO FAILURE FOR VARIATIONS IN TEMPERATURE, AND ALLOWABLE STRESS AT TWO DIFFERENT HEATING TIMES INCLUDING EFFECTS OF TRANSIENT HEATING

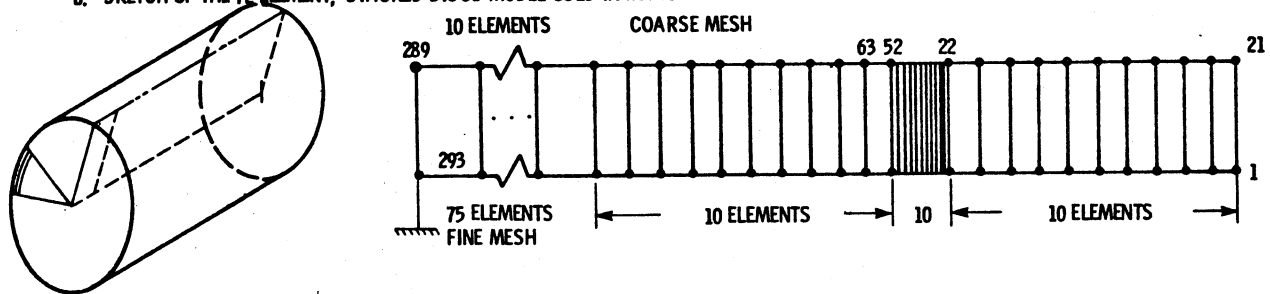
Allowable stress	Number of 3-minute cycles to failure		Experimental 24-specimen data set (ref. 7)	Number of 57-minute cycles to failure		Experimental 4-specimen data set (ref. 2)
	Calculated at inter-face temperature-			Calculated at inter-face temperature-		
	1283 K (1850° F)	1311 K (1900° F)		1283 K (1850° F)	1311 K (1900° F)	
$\sigma_p = \bar{\sigma}_p - S_0$	920	15	810	---	--	50
$\sigma_p = \bar{\sigma}_p$	$2.1 \times 10^4$	335	1330	265	4	180
$\sigma_p = \bar{\sigma}_p + S_0$	$8.6 \times 10^4$	1375	1870	1230	20	250



a. SKETCH OF THE 18 AND 66 ELEMENT MODELS USED IN ADINA AND ADINAT



b. SKETCH OF THE 72 ELEMENT, STACKED DISCS MODEL USED IN MARC



c. SKETCH OF THE 40 AND 105 ELEMENT MODELS USED IN SINDA-FEATS

Figure 1 - Finite element idealization of a multilayered cylindrical rod, thermal loading.

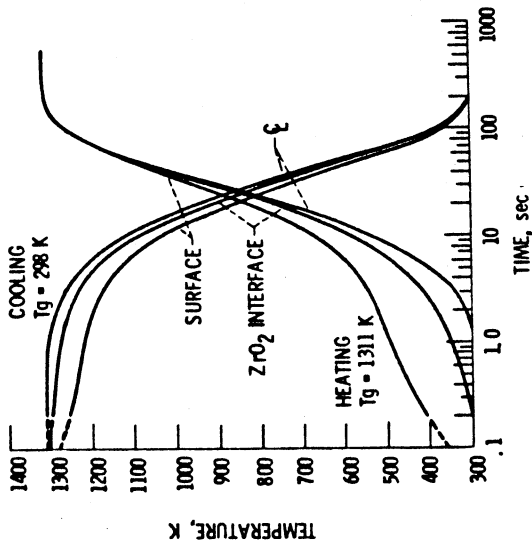


Figure 2. - Temperature distribution in the cylindrical rod during the heat cycle, calculations by ADINAT.

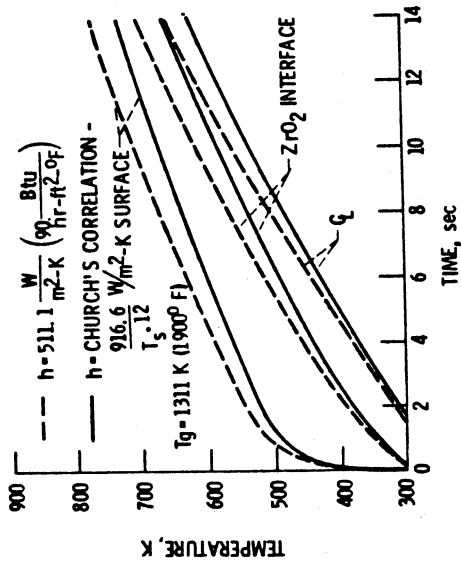


Figure 3. - Comparison of the temperature distributions based on two different heat transfer coefficient correlations, calculations by ADINAT.

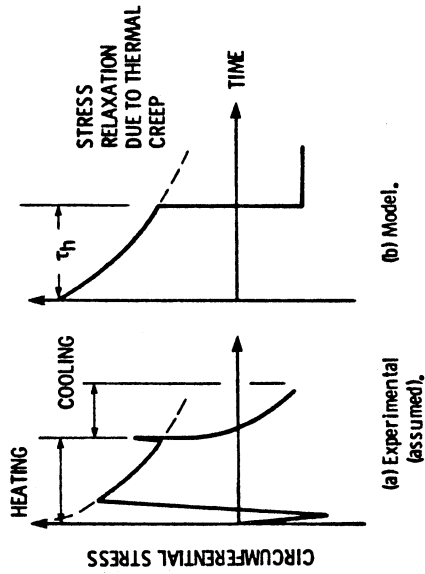


Figure 4. - Sketch of the assumed stress-time relations for a ceramic coated cylinder exposed to a 0.3 mach burner flame.

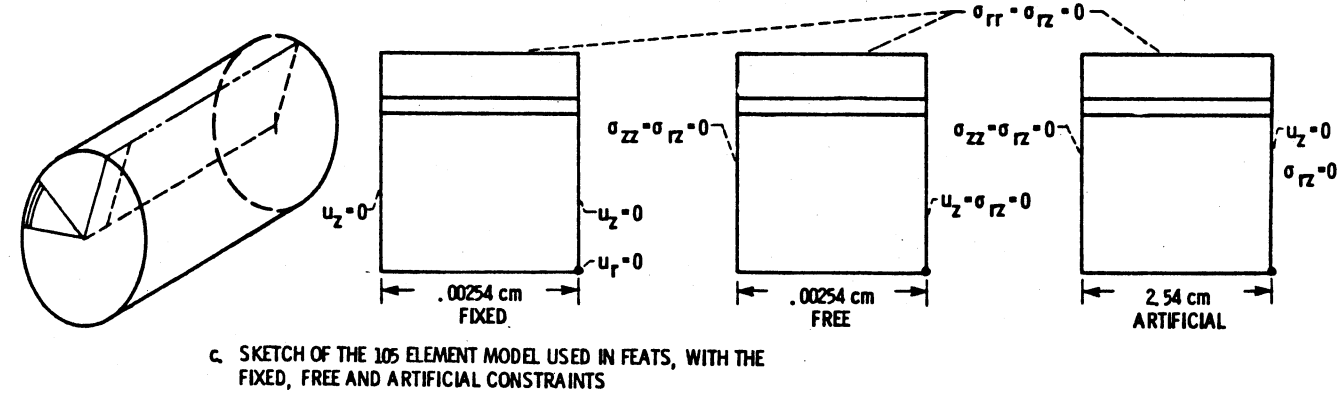
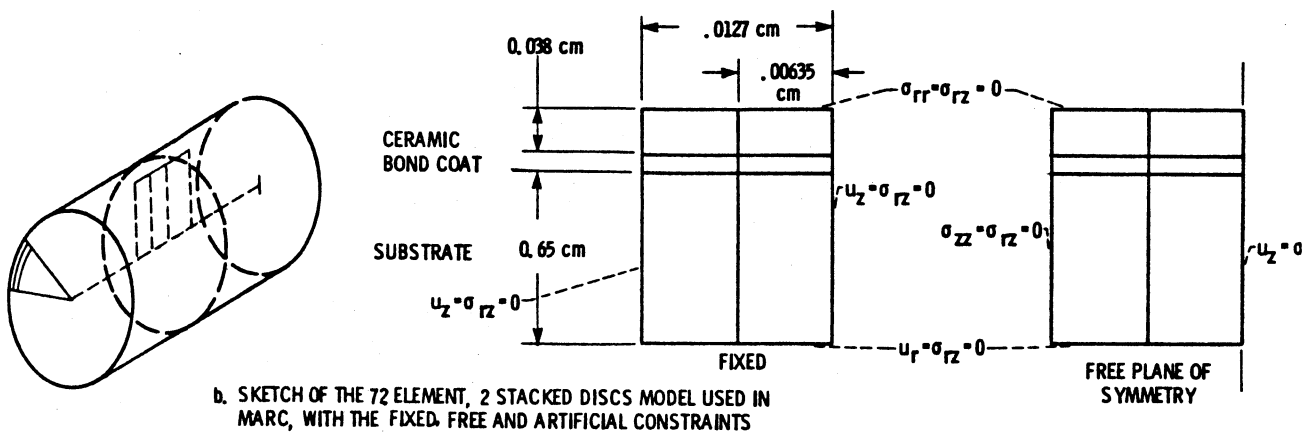
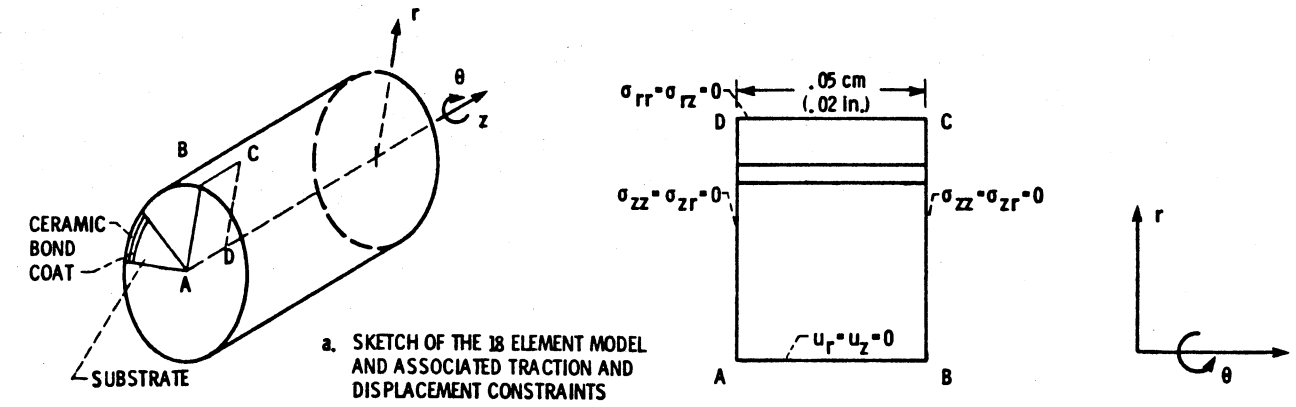


Figure 5. - Finite element idealization of a multilayered cylindrical rod, mechanical loading.

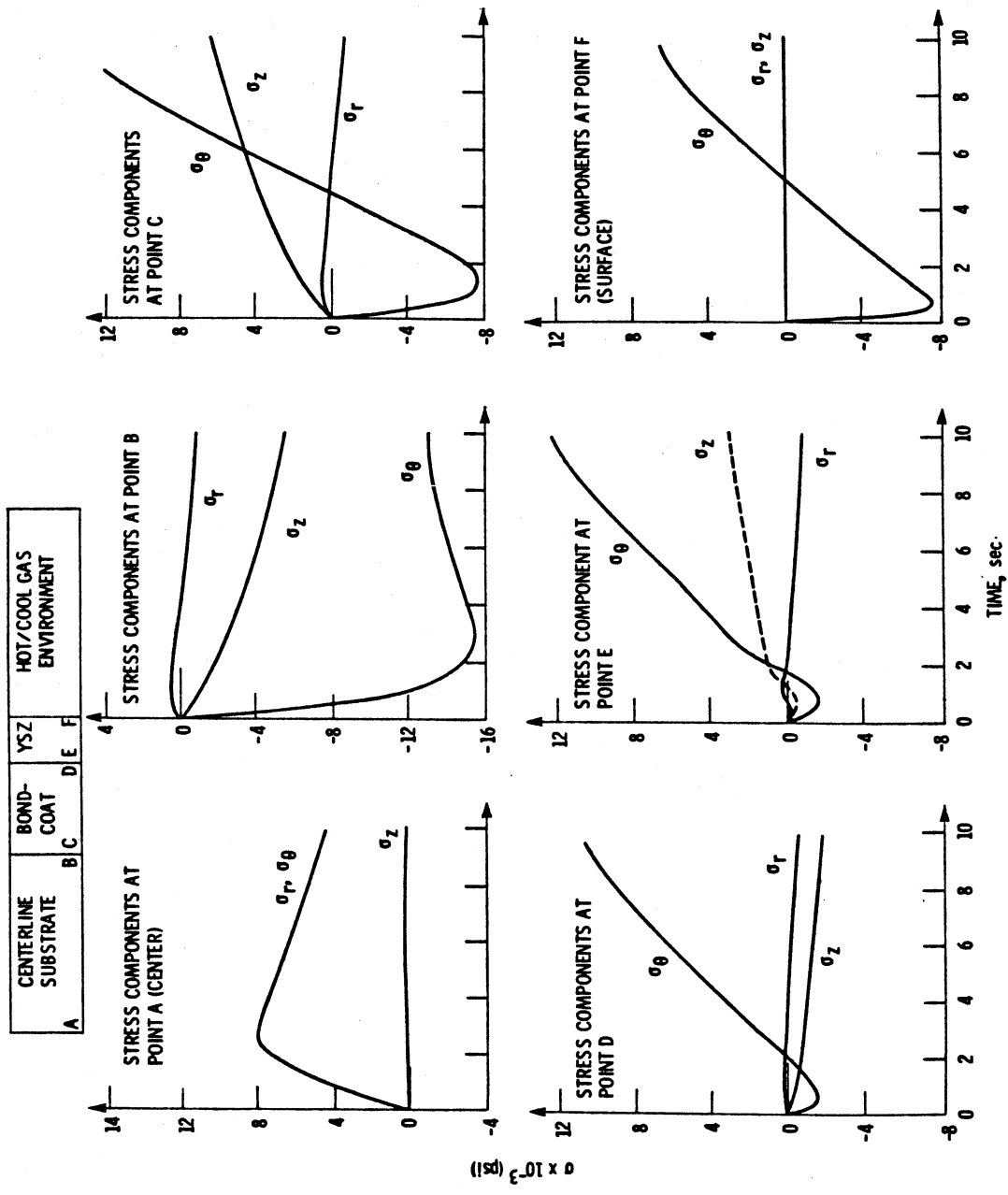


Figure 6. - Stress distributions in a multilayered cylindrical rod subjected to the thermal and mechanical loadings of sections 3 and 4, ADINA.

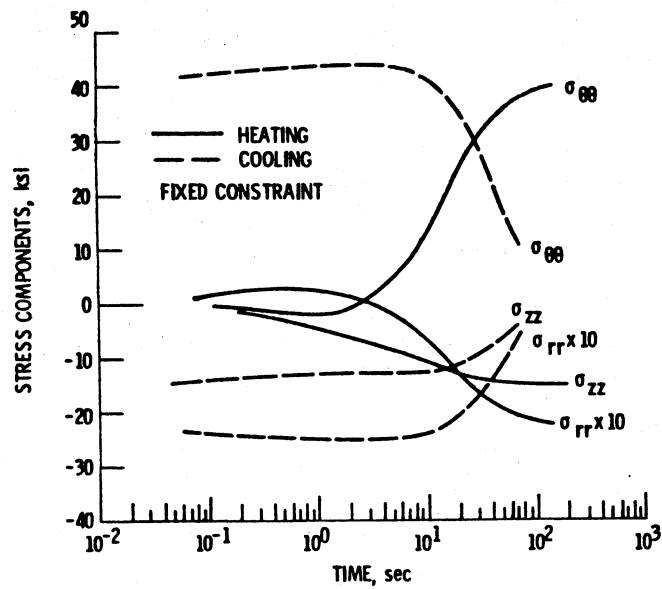


Figure 7. Stress-time distributions at location E, the bondcoat-ceramic interface for the thermal and mechanical loadings of sections 3 and 4 with fixed end constraint, MARC.

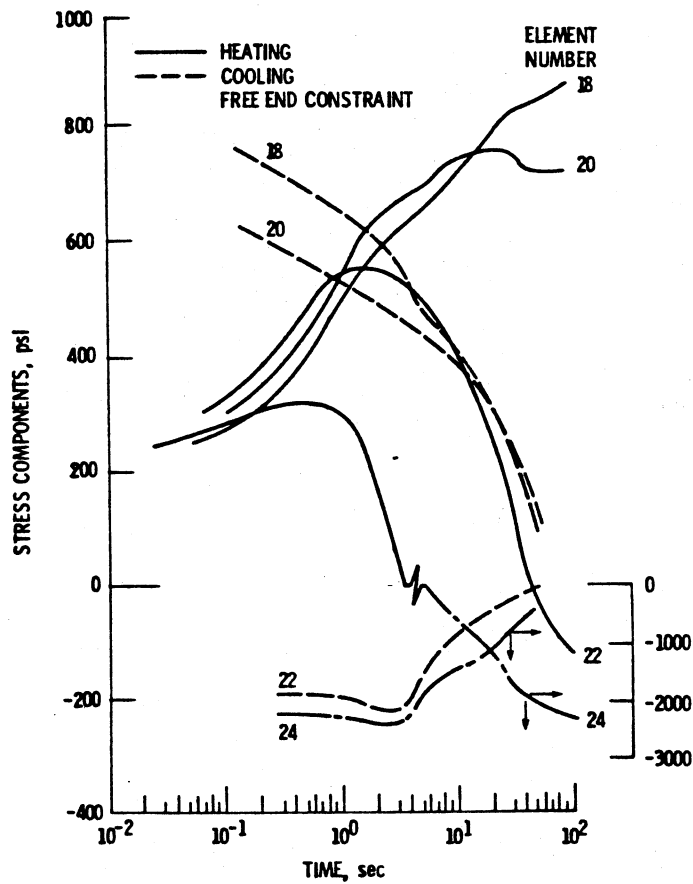


Figure 8. - Radial stress-time distributions for elements adjacent to the plane of symmetry for the thermal and mechanical loadings of sections 3 and 4 with a free end constraint, MARC. See Fig. 1 (b) for element numbers.

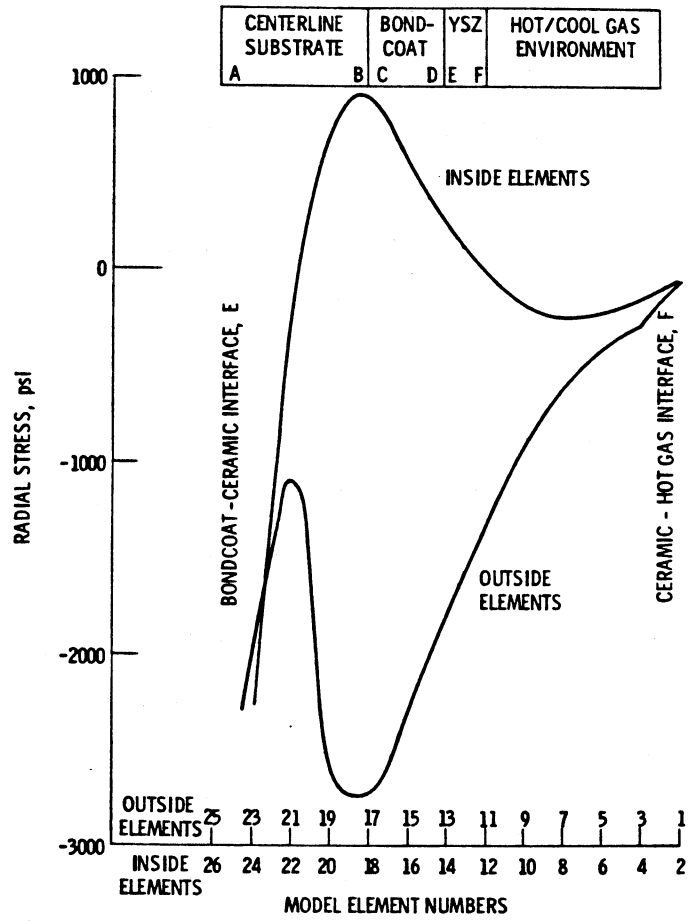


Figure 9. - Radial stress distribution for elements adjacent to the plane of symmetry (inside elements) and those on the surface (outside elements). See Fig. 1 (b) for element numbers.

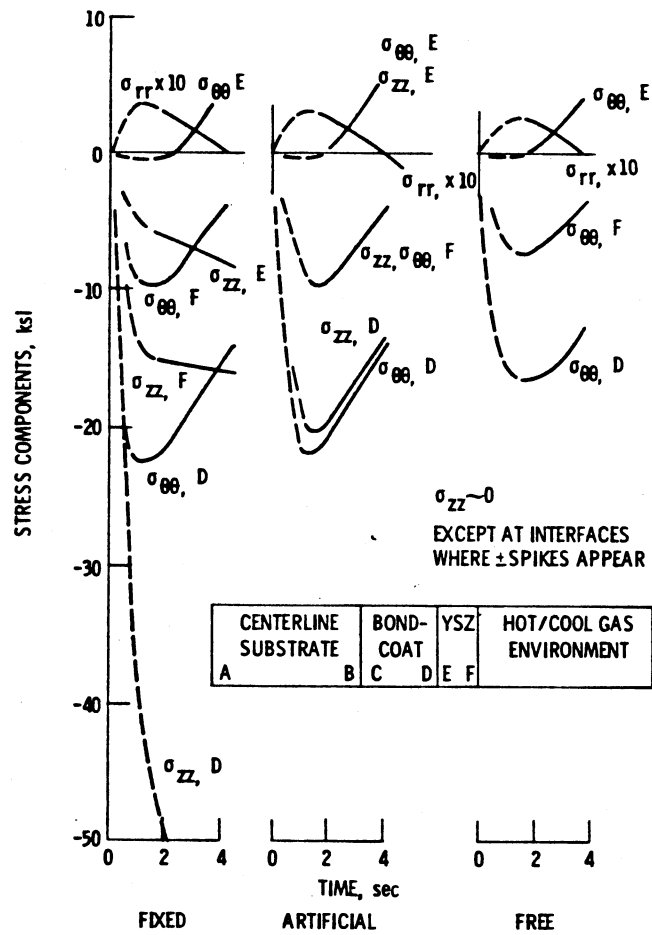


Figure 10. - Stress-time distributions for free, fixed, and artificial end constraints.

1. Report No. <b>NASA TM-83312</b>	2. Government Accession No.	3. Recipient's Catalog No.	
4. Title and Subtitle <b>THERMOMECHANICAL LOADING OF MULTILAYERED CYLINDRICAL GEOMETRIES IN THERMAL CYCLING FROM 300 TO 1300 K</b>		5. Report Date	
		6. Performing Organization Code <b>505-33-52</b>	
7. Author(s) <b>R. C. Hendricks, G. McDonald, R. L. Mullen, M. J. Braun, B. T. Chung, and J. Padovan</b>		8. Performing Organization Report No. <b>E-1518</b>	
		10. Work Unit No.	
9. Performing Organization Name and Address <b>National Aeronautics and Space Administration Lewis Research Center Cleveland, Ohio 44135</b>		11. Contract or Grant No.	
		13. Type of Report and Period Covered <b>Technical Memorandum</b>	
12. Sponsoring Agency Name and Address <b>National Aeronautics and Space Administration Washington, D. C. 20546</b>		14. Sponsoring Agency Code	
		15. Supplementary Notes <b>R. C. Hendricks and G. McDonald, NASA Lewis Research Center; R. L. Mullen, Case Western Reserve University, Dept. of Civil Engineering, Cleveland, Ohio 44106; M. J. Braun, B. T. Chung, and J. Padovan, University of Akron, Dept. of Mechanical Engineering, Akron, Ohio 44325. Prepared for the Thermal Engineering Joint Conference cosponsored by the American Society of Mechanical Engineers, Honolulu, Hawaii, March 20-24, 1983.</b>	
16. Abstract <p>The principle of multiple material layering is well known as an effective method of reducing heat transfer; however, thermal gradients can impose significant mechanical loads and lead to delamination and subsequent component failure. An analysis is developed and experimental data are discussed for the thermomechanical effects of multilayered materials on a heat sink substrate of cylindrical geometry subject to thermal cycling. The geometry is heated in cross-flow by a high-velocity flame and cooled in crossflow by ambient-temperature air from a critical flow orifice. Each layer of material possesses a threshold beyond which small changes in temperature or mechanical loading greatly influence the life in thermal cycling of the layered materials. Comparisons are made between the thermomechanical loads predicted by various numerical codes for the linear case and by a simplified analytic model.</p>			
17. Key Words (Suggested by Author(s)) <b>Seal; Ceramic; Coating; Thermomechanical; Thermal cycling</b>		18. Distribution Statement <b>Unclassified - unlimited STAR Category 34</b>	
19. Security Classif. (of this report) <b>Unclassified</b>	20. Security Classif. (of this page) <b>Unclassified</b>	21. No. of Pages	22. Price*